

# A circumstellar dust disk around a star with a known planetary companion

David E. Trilling & Robert H. Brown

Lunar and Planetary Laboratory, University of Arizona,  
1629 East University Boulevard, Tucson, Arizona 85721, USA

A planet with a minimum mass of 0.84 Jupiter masses ( $M_J$ ) has been indirectly detected<sup>1</sup> in a close orbit (radius 0.11 astronomical units, period 14.65 days) around the star 55 Cancri, which is of spectral type G8 and about 3 billion years old. The detection of excess infrared emission from this system also suggests<sup>2</sup> the presence of circumstellar dust. Our Solar System has a disk of dust (and larger bodies) that is roughly coplanar with the planets—the so-called Kuiper Belt<sup>3</sup>. Here we report infrared coronagraphic observations of 55 Cancri in which the light from the primary star is blocked, allowing us to image a circumstellar dust disk. We find that the dust lies in a disk that extends to at least 40 AU, comparable to the expected extent for our Kuiper Belt<sup>3</sup>, whereas the inferred mass of the disk is approximately ten times that estimated for our Kuiper Belt. The disk around 55 Cancri is relatively dark at a wavelength of 2.3  $\mu\text{m}$ , which is consistent with absorption of light by methane ice on the dust particles. Assuming that the disk is coplanar with the planet, we determine the planet's mass to be  $1.9^{+1.1}_{-0.4}$  Jupiter masses. All the available evidence is suggestive of a mature planetary system around 55 Cancri.

Using the CoCo cooled coronagraph with NSFCAM on NASA's Infrared Telescope Facility (IRTF) on Mauna Kea, we searched the 55 Cancri (55 Cnc,  $\rho^1$  Cnc, HD 75732, HR 3522, G8V, 12.53 pc (ref. 4)) system for evidence of circumstellar material. CoCo is a cryogenically cooled infrared Lyot coronagraphic front end to NSFCAM, and uses a gaussian apodized focal plane mask with selectable and articulatable Lyot stops. The coronagraph acts as a two-dimensional Fourier filter, blocking light from the central star as well as light diffracted from the edges of the primary mirror and Cassegrain hole, while allowing imaging to within 18 AU of 55 Cnc. The coronagraphic technique was first used to image circumstellar disks for the Beta Pictoris disk, the first directly imaged circumstellar disk<sup>5</sup>. In these observations, the residual stellar-halo intensity is at most one-tenth of that without the coronagraph. The data reduction requires subtracting the scaled stellar haloes of comparison stars (that are of similar spectral type and magnitude and are nearby on the sky) from the observed stellar halo of 55 Cnc. Halo subtraction was performed on 55 Cnc data by using each of three comparison stars to eliminate the effects of potential anomalies from any one comparison star. This technique (one object star, three comparison stars) was repeated for each of our three filters (H, K' and methane, with central wavelengths of 1.62, 2.12 and 2.28  $\mu\text{m}$ , respectively).

Our final image is shown in Fig. 1. We find a flux excess, not attributable to residual stellar halo, to the northeast and southwest (major-axis direction) of the star, and a smaller flux excess to the northwest and southeast (minor-axis direction) of the star. This signal is most pronounced in the H filter (Fig. 1a), where the signal-to-noise ratio is more than 100; in the K' filter, the signal-to-noise ratio is  $\sim 50$ . Excess circumstellar flux is detected at a very low level ( $\sim 3\text{--}5\sigma$ ) in the methane filter. Low signal in the methane filter is consistent with absorption of light at that wavelength by surfaces composed at least partly of methane ice<sup>6</sup>. Figure 1b shows the H filter data, contoured, with the best-fit ellipse overplotted to accentuate the geometry of the disk. We achieved an H-band sensitivity of  $10^{-5}$  for the ratio of the circumstellar disk flux to the peak intensity of the central star.

We performed a series of tests to ensure that our detected signal was not produced by any systematic error. We have imaged several K-dwarf stars under similar conditions, with the same instrumental configuration, and found no excess flux in any direction beyond the coronagraphic mask. We also imaged a circumstellar disk (MWC480) with known inclination on the sky<sup>7</sup> and reproduce the known inclination (nearly face-on). We find no evidence of asymmetric flux from the disk around MWC480, thus indicating that any asymmetry detected in the flux from 55 Cnc is endemic to that system only. All this evidence demonstrates that neither the telescope (focus, tracking), the instrumentation, nor the presence of any nearby stars introduced any kind of asymmetric flux excess or bias, and that our data reduction techniques are free of systematic errors that could produce the kind of signal we detected. Comparing the images of 55 Cnc with those of several different standard stars reveals the same asymmetry in all final results; intercomparing two standard stars by the same technique reveals no asymmetries. We therefore believe that the northeast–southwest asymmetric flux excess seen around 55 Cnc is real.

The radial profiles of the disk flux show a power-law dependence with a power law index of  $-5$  to  $-5.5$  (Fig. 2). This index is consistent with light reflected off a population whose spatial extent is similar to that expected for our Kuiper Belt, as solar flux decreases with distance as  $r^{-2}$  and the surface density of objects in the Kuiper Belt is estimated to fall off approximately as  $r^{-3}$  (ref. 8). Because the signal we detect is light from the central star reflected off dust particles, we can determine a rough relative reflectance spectrum for the circumstellar material (Fig. 3). We find that the material we

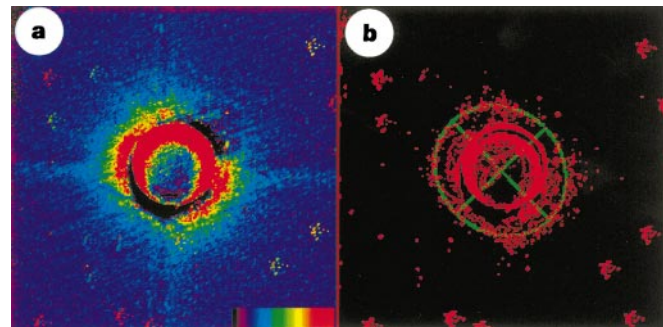


**Figure 1** Infrared coronagraphic imaging of circumstellar material around 55 Cnc. **a**, H filter image, 58 min total integration time (29 coadds of 2-min exposures). **b**, H filter total image, contoured, with best-fit ellipse and major and minor axes overlaid. The circle in the centre of the image is the coronagraphic mask, which has a diameter of 3 arcsec. The image is  $\sim 15$  arcsec on a side at a plate scale of  $\sim 0.06$  arcsec per pixel. North is up and east is to the left. The faint vertical and horizontal lines emanating from the coronagraphic mask are the remnants of the diffraction patterns of the telescope spiders, which are used to help to register images. The repeating pattern of spots represents cosmic ray hits in the flat field frame; the clusters result from the slight, repeated shifts used in co-aligning the coronagraphic images, causing a cosmic ray hit to show up as a cluster in the fully processed data. The colour bar in the lower right of **a** has a range of 0–1.81 mJy arcsec $^{-2}$ , with a linear colour map applied in this image. The contour interval in **b** is 0.83 mJy arcsec $^{-2}$ , with a lowest contour of 1.11 mJy arcsec $^{-2}$ . The ellipse is roughly fitted to the outermost contour drawn in this image. (1 Jy (Jansky) =  $10^{-12}$  W m $^{-2}$   $\mu\text{m}^{-1}$  at H band.) The coronagraph blocks light from the central star while allowing imaging to within 1.5 arcsec, or 18 AU for 55 Cnc, of the central star. Interspersed with 55 Cnc observations were observations of comparison stars. All observations were made at less than 2 airmasses, and most observations at less than 1.5 airmasses. Images are sky-subtracted and flat-fielded. A 55 Cnc image was then aligned with a comparison star image, the fluxes were scaled, and the comparison star was subtracted from object star (55 Cnc). In this way, the residual stellar halo was removed from the 55 Cnc images, on the basis of the assumption that the residual stellar halo is simply an expression of the point spread function (PSF), and that the PSF is nearly identical for a nearby comparison star for observations taken at nearly the same time.

detected has a spectrum similar to that of Pluto, often considered the largest and best studied Kuiper Belt object in our Solar System<sup>9</sup>. In particular, the relative reflectance spectra for both the 55 Cnc disk material and Pluto show a drop in reflectance at  $\sim 2.32 \mu\text{m}$ , where methane ice absorbs photons. Pluto's spectrum returns to a continuum value towards longer wavelengths than the methane ice absorption feature. However, we do not have data for the 55 Cnc circumstellar disk at wavelengths longer than  $2.32 \mu\text{m}$ , so we can at best say that the spectrum of the disk material is consistent with the presence of a methane ice absorption feature at  $2.32 \mu\text{m}$ . This spectral signature is consistent with a theoretical extrasolar Kuiper Belt, because methane ice and water ice would be expected to be present at those distances, by cosmochemical arguments<sup>10</sup>. Further study of extrasolar Kuiper Belts might prove very useful in discussing circumstellar environments and constraining global Kuiper Belt population distributions and compositions, because the global properties of an extrasolar disk can be studied and mapped in a way in which ours presently cannot.

From the radial profiles of the disk we also measure the apparent detectable extent of the disk. In the major axis direction, we confidently ( $>10\sigma$ ) detect the disk to a distance of at least 40 AU ( $3.24 \text{ arcsec}$ ) from the centre of the star, a distance which would be comfortably within our Kuiper Belt<sup>3</sup>. We measure the extent of the

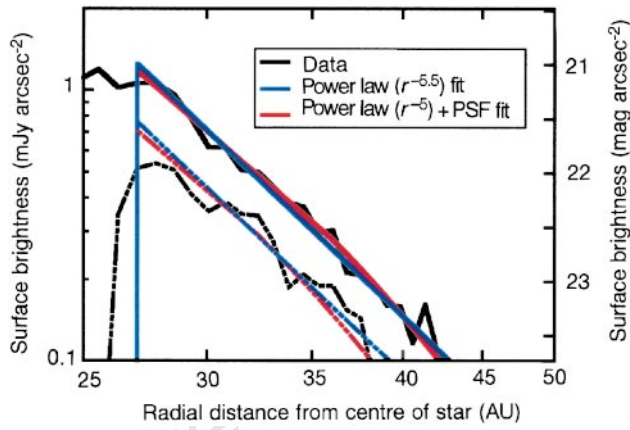


**Figure 2** Radial profiles of the disk. These H-band profiles are summed over all phase angles within the major-axis or minor-axis quadrant; the surface brightness of the disk is shown, in mJy (and magnitudes)  $\text{arcsec}^{-2}$ , in this figure. Data are shown in black, with model disks in blue and red. Solid lines represent the major-axis quadrants, and broken lines signify minor-axis quadrants. The two sets of models drawn represent two slightly different physical scenarios. The blue lines represent a simple power law, with radial dependence  $r^{-5.5}$ . The red curves represent models in which the disk has an abrupt outer edge at  $\sim 35 \text{ AU}$ . If the disk were to have this abrupt edge, the point spread function for these observations would smear the outer edge of the disk, making it seem that the disk's extent were larger than its actual size. The model fits for such a scenario are convolutions of a power law (representing the radial structure of and reflected light flux from the disk) and a gaussian with width equal to the seeing (in this case,  $0.8 \text{ arcsec}$ ), representing the observed outward smearing of the edge of the disk. The power law with the best fit in this case has a radial dependence of  $r^{-5}$ . In both models, the power-law exponents are in physical agreement with a decrease in solar flux ( $r^{-2}$ ) and a decrease in population density ( $r^{-3}$ ) (ref. 8). It is unlikely that a disk would have a truncated outer edge (red curves) without some unusual dynamical cause; it is more likely that the disk's radial structure continues (blue lines) out farther than we can detect it. Nevertheless, the two interpretations fit our data equally well. Note that the same radial functions fit the profiles in both the major-axis and minor-axis quadrants, suggesting that those quadrants represent the same physical environment, with the minor-axis direction foreshortened. Model fits begin at  $27 \text{ AU}$ , where we are fully confident that the radial extent of the coronagraphic mask is exceeded. The fluctuations from smooth in the data are known artefacts of the polar-coordinate binning that we use;  $1\sigma$  in our reduced composite frames is  $\sim 0.01 \text{ mJy arcsec}^{-2}$  for our H filter data.

semi-minor axis to be  $2.88 \pm 0.24 \text{ arcsec}$ . From these two measurements, assuming a relatively planar disk<sup>3</sup> that is circular and coplanar with the planet's orbit, we find that the inclination of the system on the plane of the sky is  $27^{+8}_{-11} \text{ }^\circ$ . Because radial velocity measurements constrain the mass of a planetary companion to be  $M_p \sin i = 0.84 M_J$  (ref. 1), we can remove the uncertainty of the planetary companion's mass by measuring the inclination of the planet's orbit on the plane of the sky. We find that the planet's mass is  $1.9^{+1.1}_{-0.4} M_J$ . The position angle of the disk's major axis is about  $50^\circ \pm 10^\circ$ .

Our detection of a disk around 55 Cnc joins other measurements (a radial-velocity companion<sup>1</sup>, the possibility of a second radial-velocity companion<sup>1</sup>, and a  $60\text{-}\mu\text{m}$  flux excess<sup>2</sup>) in indirectly suggesting the presence of a mature planetary system (one that formed from a normal protoplanetary disk and has a number of regular members) around 55 Cnc. By restricting the mass of 55 Cnc b (the planetary companion) to less than  $\sim 3 M_J$ , we eliminate the possibility that the radial-velocity companion is a brown dwarf or stellar companion, further arguing for a planetary system, not a multiple stellar system. 55 Cnc b has around one-tenth the angular momentum of Jupiter, where most of the angular momentum in our Solar System resides. If, as is assumed, the reflected light we observe from the 55 Cnc disk is primarily reflected from micro-metre-sized particles, the observations require a disk with larger surface area and hence greater mass than that of our Kuiper Belt. Assuming an average particle density of  $1 \text{ g cm}^{-3}$ , an overall near-infrared reflectance of 6%, as observed for Kuiper Belt objects in our Solar System<sup>11,12</sup>, and a collisionally evolved population of particles with a power-law index of  $-3.5$  (refs 13, 14), we find that the mass of the disk around 55 Cnc is 10 times the mass of our Kuiper Belt, to within a factor of 3. This circumstellar disk mass is consistent with the estimates of Dominik *et al.*<sup>2</sup> ( $M_{\text{disk}} > 4 \times 10^{-5} M_{\text{Earth}}$ ) as our Kuiper Belt's mass is estimated to be  $4 \times 10^{-2} M_{\text{Earth}}$  (refs 3, 8) and 55 Cnc's circumstellar disk is estimated to be more massive than that by a factor of 10. This inferred mass excess relative to our Solar System's Kuiper Belt (55 Cnc's disk being a factor of 10 more massive) is consistent with the idea that 55 Cnc b migrated inwards from its location of formation<sup>15-17</sup>. In this model, a planet migrates

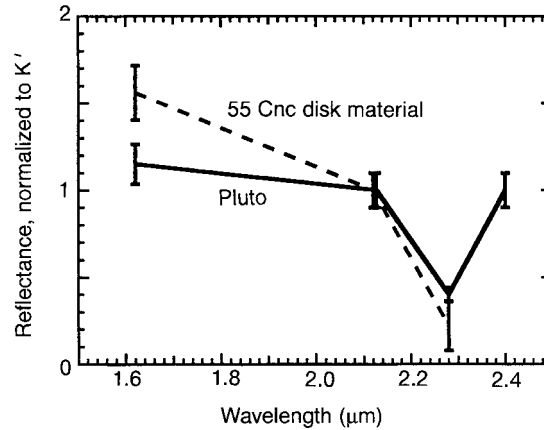


**Figure 3** Spectra of 55 Cnc circumstellar disk material and Pluto. This figure shows broadband relative reflectance of the circumstellar material around 55 Cnc and a spectrum of Pluto<sup>9</sup>. Reflectances are normalized to be equal at  $K'$ . Relative reflectances for the disk material are found by taking the ratios between images in the three filters. A decrease in reflectance at  $2.32 \mu\text{m}$  is clear in both spectra. Pluto's spectrum clearly rises back to a continuum value towards longer wavelengths than  $2.32 \mu\text{m}$ ; our data for 55 Cnc do not extend past the methane filter at  $2.32 \mu\text{m}$ . Therefore, we cannot confirm the suggested absorption feature, although our data are consistent with the presence of methane ice on the surfaces in the disk around 55 Cnc. Pluto is a relevant comparison both because of heliocentric distance (and hence surface cosmochemistry), and because Pluto is probably genetically and dynamically related to Kuiper Belt objects<sup>9,18,19</sup>.

inwards by angular momentum exchange with a protoplanetary disk (which initially extends inward nearly to the star). This migration could transfer material from the inner part of the disk to the outer part. The mass enhancement of the outer disk should be related to the angular momentum lost from the planet. Our observations are consistent with a circumstellar disk ten times more massive than our own, consistent with transfer of angular momentum from a migrating planet to the outer disk. Furthermore, the disk of material around 55 Cnc shows an extent consistent with what is expected for our own Kuiper Belt, and a spectral similarity to that expected for our Kuiper Belt. Unlike our Kuiper Belt, a disk around another star can be studied globally to determine its mass, composition and radial structure. Further study of this and other circumstellar disks will allow the characterization of global properties and will in turn lead to an increased understanding of our own Kuiper Belt. □

Received 3 April; accepted 9 July 1998.

1. Butler, R. P., Marcy, G. W., Williams, E., Hauser, H. & Shirts, P. Three new '51 Pegasi-type' planets. *Astrophys. J.* **474**, L115–L118 (1997).
2. Dominik, C., Laureijs, R. J., Jourdan de Muizon, M. & Habing, H. J. A Vega-like disk associated with the planetary system of p<sup>1</sup> Cnc. *Astron. Astrophys.* **329**, L53–L56 (1998).
3. Weissman, P. The Kuiper belt. *Annu. Rev. Astron. Astrophys.* **33**, 327–358 (1995).
4. *The Hipparcos and Tycho Catalogues* (European Space Agency, Noordwijk, The Netherlands, 1997).
5. Smith, B. A. & Terrile, R. J. A circumstellar disk around β Pictoris. *Science* **226**, 1421–1424 (1984).
6. Brown, R. H., Cruikshank, D. P., Pendleton, Y. & Veeder, G. J. Surface composition of Kuiper belt object 1993C. *Science* **276**, 937–939 (1997).
7. Mannings, V., Koerner, D. W. & Sargent, A. I. A rotating disk of gas and dust around a young counterpart to β Pictoris. *Nature* **388**, 555–557 (1997).
8. Duncan, M. J. & Levison, H. F. A disk of scattered icy objects and the origin of Jupiter-family comets. *Science* **276**, 1670–1672 (1997).
9. Owen, T. C. et al. Surface ices and the atmospheric composition of Pluto. *Science* **261**, 745–748 (1993).
10. Lewis, J. S. *Physics and Chemistry of the Solar System* (Academic, San Diego, 1995).
11. Luu, J. X. & Jewitt, D. C. Reflection spectrum of the Kuiper belt object 1993 SC. *Astron. J.* **111**, 499–503 (1996).
12. Jewitt, D. C., Luu, J. X. & Chen, J. The Mauna Kea–Cerro Tololo (MKCT) Kuiper belt and centaur survey. *Astron. J.* **112**, 1225–1238 (1996).
13. Farinella, P. & Davis, D. R. Short-period comets: primordial bodies or collisional fragments? *Science* **273**, 938–941 (1996).
14. Dohnanyi, J. S. Collisional model of asteroids and their debris. *J. Geophys. Res.* **74**, 2531–2554 (1969).
15. Lin, D. N. C., Bodenheimer, P. & Richardson, D. C. Orbital migration of the planetary companion of 51 Pegasi to its present location. *Nature* **380**, 606–607 (1996).
16. Trilling, D. E. et al. Orbital evolution and migration of giant planets: modeling extrasolar planets. *Astrophys. J.* **500**, 428–439 (1998).
17. Murray, N., Hansen, B., Holman, M. & Tremaine, S. Migrating planets. *Science* **279**, 69–72 (1998).
18. Duncan, M. J., Levison, H. F. & Budd, S. M. The dynamical structure of the Kuiper belt. *Astron. J.* **110**, 3073–3081 (1995).
19. Malhotra, R. The origin of Pluto's peculiar orbit. *Nature* **365**, 819–821 (1993).

**Acknowledgements.** We thank Doug Toomey for instrumental assistance, and Andy Rivkin for many useful discussions. D.E.T. and R.H.B. were visiting astronomers at the Infrared Telescope Facility which is operated by the University of Hawaii under contract to the National Aeronautics and Space Administration. This work is supported in part by an NSF Graduate Research Fellowship and by various NASA research grants.

Correspondence should be addressed to D.E.T. (e-mail: trilling@pl.arizona.edu).

contrast to Ganymede<sup>3</sup> and possibly Io<sup>4</sup>. Here we report perturbations of the external magnetic fields (associated with Jupiter's inner magnetosphere) in the vicinity of both Europa and Callisto. We interpret these perturbations as arising from induced magnetic fields, generated by the moons in response to the periodically varying plasma environment. Electromagnetic induction requires eddy currents to flow within the moons, and our calculations show that the most probable explanation is that there are layers of significant electrical conductivity just beneath the surfaces of both moons. We argue that these conducting layers may best be explained by the presence of salty liquid-water oceans, for which there is already indirect geological evidence<sup>5,6</sup> in the case of Europa.

Our insight into the source of the magnetic perturbations

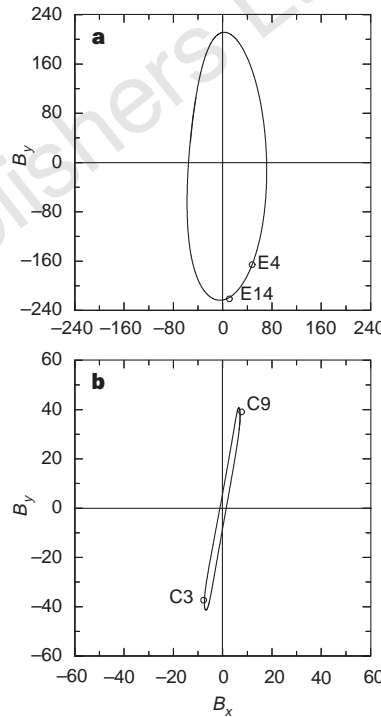


**Figure 1** The varying magnetic fields experienced by Europa and Callisto. Near the orbits of the satellites (the orbits of Europa and Callisto lie nearly in Jupiter's spin equator at  $9.4R_J$  and  $26.3R_J$ , respectively) but remote from the actual satellite locations, the sources of magnetic field are the internal tilted dipole of Jupiter and the currents flowing in the magnetospheric plasma sheet. The  $9.6^\circ$  tilt between Jupiter's spin and dipole axes implies that the magnetic equatorial plane and the orbital planes of the moons are inclined relative to each other. In a coordinate system with the  $x$  axis along the direction of plasma co-rotation, the  $y$  axis orientated towards Jupiter, and the  $z$  axis along the spin axis of the moon, the  $z$  component remains essentially constant. However, the  $x$  and  $y$  components of the magnetospheric field vary at the synodic period of Jupiter's rotation (11.1 h for Europa and 10.1 h for Callisto) as illustrated in the plots. **a**, The elliptically polarized variation of the magnetic field (in nT) at Europa. Open circles mark the field values corresponding to the E4 and E14 fly-bys. **b**, The almost linearly polarized variation of the magnetic field (in nT) at Callisto. Open circles mark the field values corresponding to the C3 and C9 fly-bys. The time, altitude and latitude relative to the moon's equator for the four passes were: E4, 1996 December 19 06:52:58 UT, 688.1 km,  $-1.6^\circ$ ; E14, 1998 March 29 13:21:16 UT, 1,641.3 km,  $12.0^\circ$ ; C3, 1996 November 04 13:24:28 UT, 1,138.9 km,  $13.2^\circ$ ; C9, 1997 June 25 13:47:50 UT, 421.0 km,  $2.0^\circ$ . At the times of these encounters, the SIII west longitude and position relative to the jovian plasma sheet were: E4,  $156.8^\circ$ ,  $\sim 1R_J$  above; E14,  $184.4^\circ$ ,  $\sim 1R_J$  above; C3,  $242.9^\circ$ ,  $\sim 1R_J$  above; C9,  $59.9^\circ$ ,  $\sim 1R_J$  below ( $R_J$  = radius of Jupiter = 71,492 km). The expected background field was calculated from an empirical model of Jupiter's magnetospheric field that uses spherical harmonics of order 3 to describe the internal field<sup>32</sup> and an Euler potential formulation<sup>33</sup> to describe the external field from the current sheet.

## Induced magnetic fields as evidence for subsurface oceans in Europa and Callisto

K. K. Khurana\*, M. G. Kivelson\*†, D. J. Stevenson‡, G. Schubert\*†, C. T. Russell\*†, R. J. Walker\* & C. Polanskey§

\* Institute of Geophysics and Planetary Physics, † Department of Earth and Space Sciences, University of California, Los Angeles, California 90095, USA

‡ Division of Geological and Planetary Sciences, California Institute of Technology, Pasadena, California 91125, USA

§ The Jet Propulsion Laboratory, 4800 Oak Grove Road, Pasadena, California 91109, USA

**The Galileo spacecraft has been orbiting Jupiter since 7 December 1995, and encounters one of the four galilean satellites—Io, Europa, Ganymede and Callisto—on each orbit. Initial results from the spacecraft's magnetometer<sup>1,2</sup> have indicated that neither Europa nor Callisto have an appreciable internal magnetic field, in**